Ab initio study of atomic hydrogen diffusion on the clean and hydrogen-terminated Si(001) surface

Jürgen Wieferink,[*] Peter Krüger, and Johannes Pollmann

Institut für Festkörpertheorie, Universität Münster, 48149 Münster, Germany

(Received 28 June 2010; published 23 August 2010)

Recent experiments have shown an unexpected diffusion behavior of hydrogen on the Si(001) surface at high temperatures and high coverages. To shed some light on this behavior, we have employed density-functional theory to investigate H diffusion on the flat Si(001) surface for different coverages with main emphasis on the high-coverage limit of Si(001) monohydride. Three basic diffusion steps, intradimer, intrarow, and interrow have been studied both for isolated H atoms on the clean Si(001) surface, as well as for isolated and paired H vacancies on the Si(001) monohydride surface. The barrier energies depend strongly on the distance between the two Si neighbors of the diffusing H atom in the transition state. We observe that an isolated vacancy is less mobile than an isolated H atom showing that the Si(001) monohydride surface is more rigid than the clean surface. Interestingly, two adjacent vacancies may transfer dangling-bond charge from one to another prior to a transition of one of them, which significantly lowers the transition barrier. We visualize the reaction mechanisms using maximally localized Wannier functions and we discuss hopping rates within the harmonic approximation to transition state theory in comparison with experimental data.

I. INTRODUCTION

The interaction of hydrogen atoms with the Si(001) surface is important both for epitaxial growth of Si layers by chemical vapor deposition,[1] as well as for passivating dangling bonds (DBs) to obtain a chemically and electronically inert surface. Additionally, it is an interesting model system for general aspects of chemical reactions at covalent surfaces in its own right.[2] The diffusion of H atoms on Si(001) is a very important aspect of this interaction because it plays a key role as the rate limiting step in the desorption of hydrogen molecules.[1]

On clean and flat Si(001) terraces, three kinds of surface diffusion processes have been discussed in the literature, namely, H hopping between Si atoms of one dimer (*intradimer*), between Si atoms of two adjacent dimers within the same dimer row (*intrarow*), and from one dimer row to a neighboring row (*interrow*).[3–11] According to theoretical studies,[3–6] the corresponding activation energies increase monotonically with the distance between the initial and final state positions of the H atom and get larger from intradimer through intrarow to interrow hopping, respectively. Video scanning tunneling microscopy (STM) experiments confirm this order of barrier heights.[10] Intradimer hops occur faster by roughly 2 orders of magnitude compared to intrarow hops for temperatures between 500 and 700 K.[7–10] Interrow diffusion, on the other hand, takes place on much longer time scales and is therefore difficult to study using video STM.[10] Thus it is generally agreed that surface diffusion at moderate temperatures is dominated by intradimer and intrarow hops whereas row changes occur almost exclusively at step edges or other defects.

Very recently, Höfer's group has applied a new technique of combined pulsed laser-induced heating and STM (Refs. 11 and 12) to examine intrarow and interrow diffusion at high temperatures.[11,13] Contrary to previous work, the authors did not start out with a clean Si(001)-(2×1) surface on which

they adsorbed atomic hydrogen at low coverage but rather heated up a Si(001)-(2×1) monohydride surface to 1400 K by a laser pulse for a few nanoseconds. Within this time scale some H_2 molecules desorb and a few H hopping events may happen. The H vacancy patterns resulting after the pulse were analyzed with STM. Schwalb *et al.*[13] have made the surprising observation that the rates for interrow hopping are only a factor of two smaller than those for intrarow hopping, much in contrast to all previous investigations carried out at much lower temperatures and H coverages. The authors concluded that interrow hopping is very well feasible far from defects and step edges within this temperature range. It has to be emphasized, however, that these studies[13] have only explored the very high hydrogen-coverage regime while most other publications have studied the diffusion of isolated hydrogen adatoms, i.e., the very low coverage regime.

The aim of this work is to study different types of surface hopping processes of H atoms on Si(001) in the very low and high hydrogen-coverage regimes using spin-polarized density-functional calculations of diffusion barriers and hopping rates. For reference, we first briefly address diffusion of isolated H atoms on a clean and flat Si(001) surface, which has been investigated in detail before.[3–11] Our main focus is then on H diffusion in the high-coverage regime of very few vacancies on a Si(001) monohydride surface. We note in passing that even higher H coverages, which are accompanied by Si dimer cleavage and which finally end up in a dihydride surface, are beyond the scope of this paper. Needless to say that H atoms can diffuse *within* the hydrogen layer on top of the monohydride surface only if there are vacant H sites. We have modeled Si(001) monohydride systems with one and with two hydrogen vacancies. The effective outcome of a hydrogen hopping step on these surfaces is equivalent to the hopping step of a hydrogen vacancy in opposite direction. To the best of our knowledge, H vacancy diffusion on Si(001) monohydride has been investigated so far only experimentally.[11,13] We additionally note that static

electronic and magnetic properties of hydrogen vacancy pairs have been addressed recently in a theoretical study.[14] Finally, we compare our calculated hopping rates for H vacancy diffusion at Si(001) monohydride with experimental data.

This work is organized as follows. The details of the calculations are described in Sec. II. The results are presented in Sec. III. The first subsection briefly addresses the diffusion of isolated H atoms on the clean Si(001)-(2×1) surface. In the second and third subsections, diffusion of a hydrogen vacancy in the top layer of Si(001)-(2×1) monohydride with one or two vacancies is discussed in some detail. Electronic properties and reaction mechanisms are described in addition to structural configurations along reaction pathways and activation energies. The diffusion barriers and hopping rates of all considered processes are discussed and compared with experiment in Sec. IV. A short summary concludes the paper.

II. METHODS

The calculations have been performed within spin-polarized density-functional theory (DFT) (Refs. 15 and 16) using the generalized gradient approximation (GGA) (Ref. 17) and norm-conserving pseudopotentials in Kleinman-Bylander form.[18] The wave functions are expanded in a Gaussian basis set with s, p, d, and s^* orbitals.[19] To reduce the basis set superposition errors, interaction energies have been calculated using an extended basis set.[20] The charge density and the local parts of the potential are represented by Fourier series, which allows us to use the efficient algorithms described in Ref. 21 to update the charge density and to calculate the Kohn-Sham matrix elements.

The Si(001) surface is modeled within the supercell approach with a partial H adlayer, six Si substrate layers, and a bottom dihydride saturation layer. In structure and path optimizations, the partial adlayer and the top five Si layers were allowed to fully relax and a vacuum layer of at least 8.5 Å was used between subsequent slabs. The interaction energies have been calculated using an extended vacuum layer of more than 12 Å. Brillouin-zone integrations have been performed using eight points for $c(4×4)$ as well as for $(4×3)$ reconstructed surface unit cells. Other unit cells have been modeled with an equivalent point density.

We have implemented the quadratic string method of Burger and Yang[22] for finding reaction pathways. While this method generally converges rapidly, it does not perform well with spring forces and uses other means to ensure equispacing of the images. Therefore, a combination with a climbing image[23] is not advisable for calculating transition geometries. Instead, we apply "geometry optimization by direct inversion in the iterative subspace" (GDIIS) (Refs. 24 and 25) to the climbing image force field of Ref. 23, i.e., to the path as a whole. Farkas and Schlegel[25] have added some precautions to the original GDIIS (Ref. 24) in order to converge to stable solutions, which is of paramount importance for path optimizations. Just like the quadratic string method, the GDIIS allows one to use chemically motivated models[26] for the initial guess of the second derivative of the total energy of each image.
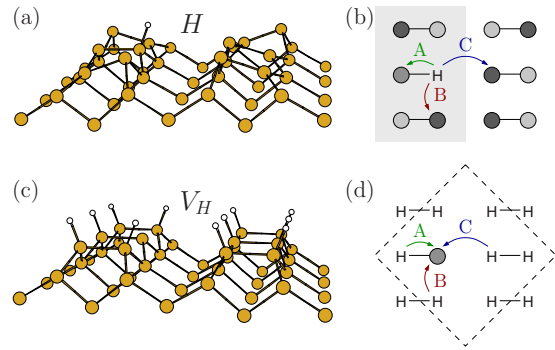
FIG. 1. (Color online) [(a) and (b)] An isolated H atom on a clean Si(001) surface and [(c) and (d)] a H vacancy ($V_{\rm H}$) on the monohydride surface. The actual geometries are shown in panels (a) and (c) with large ocher (gray) Si atoms and small white H atoms. Panels (b) and (d) are schematic top views with the unsaturated Si atoms shown as gray circles. In case of a tilted dimer, the up and down atoms are depicted as dark and bright circles, respectively. The arrows in panels (b) and (d) indicate intradimer (A), intrarow (B), and interrow (C) hops. The shaded area in panel (b) is a (2 ×3) unit cell whereas the whole sketch represents a (4×3) cell. The rotated dashed square in panel (d) is a $c(4×4)$ unit cell.

Hopping rates have been calculated within the harmonic approximation to transition state theory (hTST).[27] They follow an exponential Arrhenius behavior. Pre-exponential factors are determined from the force constant matrices at the initial and the transition geometries. These matrices are obtained using finite differences of forces.

We have also analyzed the one-particle electronic structure using maximally localized Wannier functions[28] calculated with WANNIER90.[29] The centers of mass of the Wannier functions, i.e., the expectation values of the position operator, are of special usefulness for the interpretation of the electronic properties because they depict bond positions and orders by acting as a link between related atoms. For a more detailed discussion see Ref. 30.

III. RESULTS

We first describe the diffusion of an isolated H atom on the clean Si(001) surface, for reference. That system will be denoted as H, for shortness sake. In Sec. III B, the complementary system of an isolated H vacancy diffusing in the top layer of Si(001) monohydride, denoted as $V_{\rm H}$, is investigated. The diffusion of a hydrogen vacancy on a monohydride surface with two vacancies, which we label $V_{\rm 2H}$, is addressed in Sec. III C.

A. Isolated hydrogen atom

The clean Si(001)-(2×1) surface features Si surface dimers which are relatively short (2.35 Å) and strongly buckled. The dangling bonds on the dimer atoms give rise to two DB bands which reduce the projected bulk band gap from the GGA value of 0.79 to 0.34 eV. Adsorption of a single H atom on one of the DBs leads to the structure shown in Fig. 1(a). The Si dimer with the adsorbed H atom turns out to be longer (2.40 Å) and basically unbuckled in the opti-

TABLE I. Calculated structural parameters (in Å) and activation energies ΔE_{act} (in eV) characterizing the transition states T for intradimer (A), intrarow (B), and interrow (C) hopping of an isolated H atom diffusing on the clean Si(001)-(2×1) surface. For the definition of the structure parameters, see text. The corresponding structure parameters of the initial state, i.e., for a single H atom on only one of the dimers in the unit cell [see Fig. 1(a)] are given in parentheses, for reference.

		d_{di}	$d_{H\text{-}Si}$	$d_{Si\text{-}Si}$	ΔE_{act}
H	T_A	2.30 (2.40)	1.78 (1.50)	2.30 (2.40)	1.36
	T_B	2.39 (2.40)	1.86[a] (1.50)	3.24 (3.82)	1.58
	T_C	2.56 (2.40)	2.01 (1.50)	3.91 (5.14)	2.09

[a]The two H-Si distances in the transition geometry for intrarow diffusion are different. The shorter one is given.

mized geometry with a H-Si bond length of 1.50 Å. The DB band originating from the second Si atom of this dimer is split into an occupied spin-up and an empty spin-down band, neither of which reduces the fundamental surface band gap.

We have studied three basic diffusion steps of a hydrogen atom on this surface, as indicated by the hopping processes A, B, and C in Fig. 1(b). In case A, the H atom hops from one to the other Si atom of the same dimer. In processes B or C it hops from a Si atom of one dimer to a nearest Si atom of another dimer in the same (B) or in an adjacent (C) dimer row, respectively. Thus, A is an intradimer, B an intrarow, and C an interrow hopping process. Since intradimer and intrarow hops take place within a single dimer row, they have been studied using 2×3 unit cells, comprising one row with two clean dimers and one dimer with a H atom and a free DB. The interrow hops have been modeled using a larger 4×3 unit cell. The respective unit cells are shown in Fig. 1(b).

It is worth noting at this point that the total energy depends sensitively on the precise buckling pattern of the surface. It has turned out from our calculations that hops of H atoms to Si dimer up atoms are more favorable than hops to Si dimer down atoms. Therefore, we have employed precisely the pattern shown in Figs. 1(a) and 1(b) for interrow and the left half of it for intradimer and intrarow hops. This choice additionally ensures equivalent buckling patterns for the initial and the final geometries and provides both a Si up and down atom in the vicinity of the H atom along the row so that reaction mechanisms requiring one of those can actually work.

The calculated pathways of the distinct hopping steps show significantly different surface relaxations. This is obvious in Table I where we have summarized the most important parameters characterizing the transition states. These are the bond length of the Si dimer d_{di}, the distance of the H atom and its two nearest Si neighbors in the transition state $d_{H\text{-}Si}$, as well as the distance of the latter in the transition state $d_{Si\text{-}Si}$. Note that H and its two Si neighbors in first approximation form a symmetric, isosceles triangle in the transition state. The activation energies ΔE_{act} for all three hopping kinds are also given in Table I.

In the intradimer transition state T_A the dimer bond length d_{di} and the distance $d_{Si\text{-}Si}$ are identical by definition. They are shortened to 2.30 Å while the H-Si distance $d_{H\text{-}Si}$ increases to 1.78 Å. The relaxations are particularly large for intrarow

(B) and interrow (C) hopping, where $d_{H\text{-}Si}$ and $d_{Si\text{-}Si}$ deviate the strongest in the transition states from their related initial state values. Actually, the increased d_{di} as well as the decreased $d_{Si\text{-}Si}$ values considerably reduce the hopping distance in the transition state, as compared to the initial state configuration, thus allowing for H diffusion in the first place. The intrarow transition geometry T_B is somewhat special in two respects. First, the dimers move toward each other perpendicular to the dimer direction [cf. Fig. 1(b) and the related $d_{Si\text{-}Si}$ value] so that d_{di} is not stretched. Second, the transition geometry turns out to be unsymmetric and the two H-Si distances differ from each other ($d_{H\text{-}Si}$=1.86 Å and 1.97 Å instead of 1.91 Å as resulting from a symmetry-constrained path optimization). The reduction of the symmetry lowers the corresponding activation energy ΔE_{act} from 1.65 to 1.58 eV by a charge redistribution between the two DBs on the other side of the two dimers. A more detailed discussion of the surface relaxations in the different transition states for low hydrogen coverage may be found in Ref. 3. Our results for atomic H diffusion on the clean Si(001)-(2×1) surface are in good accord with these investigations.

The barrier energies resulting from our calculations for the transition states of the investigated hopping processes are compared with results from previous theoretical and experimental studies in Table II. Our results corroborate the general trend of increasing barrier heights from intradimer through intrarow to interrow hopping. This trend is closely related to the increasing distance $d_{Si\text{-}Si}$ in the transition states (cf. Table I). When it comes to quantitative details, there are significant differences between most of the theoretical results, though, which we attribute to the diversity of methods in use. Our results can most meaningfully be compared with those of Bowler *et al.*,[10] who have studied intrarow hopping employing a similar spin-polarized GGA slab approach. Their activation energy agrees very well with our result. Actually, if we enforce a higher symmetry in the transition state T_B, i.e., if we force both H-Si distances to be the same, as assumed most probably in Ref. 10, we also find a barrier energy for intrarow hopping of 1.65 eV, as noted before.

The only experimental values in Table II are the ones by Hill *et al.*[9] The authors performed video STM within a temperature range from 450 to 650 K and fitted the activation energies to an Arrhenius behavior of the hopping rates. While our intrarow barrier energy is in good accord with

TABLE II. Calculated barrier energies (in eV) for the three different basic hopping steps of an isolated H atom on a clean Si(001)-(2×1) surface. Local density approximation (DFT-LDA) and DFT-GGA (PW91 and B3LYP functionals), as well as parameterized tight binding (TB) and force field (FF) calculations have been reported in the literature. For comparison, the first line shows our DFT results from spin-resolved GGA calculations (cf. last column of Table I) and the experimental data from video STM measurements is given in the last line.

	Intradimer (A)	Intrarow (B)	Interrow (C)
GGA-PW91-slab, this work	1.36	1.58	2.09
GGA-PW91-slab (Ref. 10)		1.65	
LDA-slab (Ref. 3)	1.2	1.3	1.8
FF-slab (Ref. 4)	1.58	1.65	2.73
FF-slab (Ref. 6)	1.1	1.8	2.4
TB-cluster (Ref. 10)	1.44	1.65	2.38
B3LYP-cluster (Ref. 5)	1.87	2.39	3.12
Expt.: STM (Ref. 9)	1.01	1.75	

experiment, the intradimer barrier determined from the experimental results is significantly smaller than the one calculated within this work. This deviation will be discussed in Sec. IV B along with a comparison of experimental and theoretical hopping rates.

B. Isolated hydrogen vacancy

Let us next address the Si(001)-(2×1) monohydride surface with a single hydrogen vacancy, i.e., the V_H system. The surface geometry of the ground state is shown in Figs. 1(c) and 1(d). It has been modeled using a $c(4×4)$ surface unit cell as indicated in Fig. 1(d). The Si dimer with the free DB is of approximately the same length (2.40 Å) as H-saturated dimers (2.41 Å) and nearly unbuckled with a tilt angle of 0.3° only. The band originating from the unsaturated DB is split into an occupied spin-up band near −0.3 eV relative to the edge of the valence bands and an unoccupied spin-down band, which reduces the gap to 0.58 eV. There are no other bands of surface states in the bulk band gap because all other dimers are hydrogen saturated.

Hopping of a H atom to the position of the vacancy on the monohydride surface can be regarded as the inverse hopping of the vacancy to the former position of the H atom. Also for vacancy diffusion, the same three basic steps of intradimer (A), intrarow (B), and interrow (C) hopping apply, as indicated in Fig. 1(d). *De facto*, they now involve hopping of

three different H atoms, which we cannot discern, however, anyway. The results for the corresponding transition-state parameters following from the respective path optimizations are summarized in Table III. By and large, the parameters of the intradimer and intrarow transition states T_A and T_B are very similar to those in the case of the isolated H atom (cf. Table I). The transition state T_C shows salient differences to the case of isolated H hopping, however. In particular, the H-Si distance in the transition state $d_{H\text{-}Si}$ deviates more from its ground state value and the transition-state distance $d_{Si\text{-}Si}$ is considerably closer to the ground state value in the V_H system than it was in the H system. As a consequence, the related activation energy is 0.25 eV larger in the V_H than in the H system indicating that the monohydride surface is stiffer than the clean Si(001)-(2×1) surface.

Concerning the electronic properties of the three transition-state configurations we note that all three transition geometries—just like the ground state—are semiconducting and spin polarized. Because of the gap, band occupancy is well defined throughout the Brillouin zone so that Wannier functions can be used to study the occupied electronic orbitals. The distribution of the Wannier functions in the ground-state geometry is visualized by the positions of their centers of mass in Fig. 2(a). The dimer bond and the two H-Si bonds of the front dimer are made up by three spin-paired Wannier functions whose centers are positioned on the bond lines. This way, each of them signals the presence of a single bonding orbital. At the DB of the back dimer, there is only a spin-up Wannier function (circle with an arrow). The centers of the two spin components of the dimer bond Wannier functions near the DB do not coincide completely because the spin-up component is "repelled" from the spin-up DB as a result of the localization procedure.

Figures 2(b) and 2(c) show the configurations of the transition states T_A and T_B, respectively. In both cases, the H atom is midway between the two involved Si atoms to which H is bonded in the initial and final state and has taken the spin-down H-Si bond electron along. Both the spin-up electrons at the two Si atoms can be viewed as DBs with partial H-Si bonding character. This interpretation is supported by the respective Wannier function of the intradimer transition state T_A in the upper panel of Fig. 2(d). We note that there is another degenerate spin-up state whose plot would be a mirrored version of the left spin-up state. Thus, effectively a neutral H atom is transferred both in intradimer and intrarow pathways, leaving a singly occupied Si DB behind. Since the interrow hopping mechanism is essentially the same it is not described in detail here for the sake of brevity.

TABLE III. Same as Table I (see caption for details) but for H diffusion on Si(001) monohydride with one vacancy.

		d_{di}	$d_{H\text{-}Si}$	$d_{Si\text{-}Si}$	ΔE_{act}
V_H	T_A	2.34 (2.40)	1.77 (1.50)	2.34 (2.40)	1.40
	T_B	2.41 (2.40)	1.95 (1.50)	3.27 (3.85)	1.76
	T_C	2.59 (2.40)	2.23 (1.50)	4.30 (5.29)	2.34
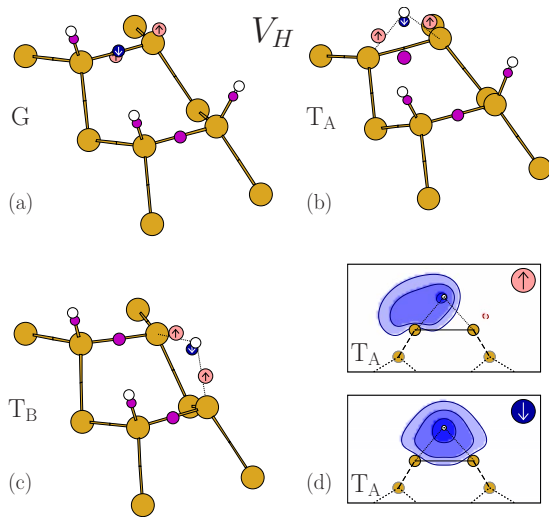
FIG. 2. (Color online) Bird's eye views of small sections of (a) a V_H ground state configuration G as well as corresponding (b) intradimer and (c) intrarow transition geometries T_A and T_B, respectively. Atoms and bonds are depicted in the same way as in Fig. 1. The centers of mass of the Wannier functions, i.e., the expectation values of the position operator, are included as additional circles. If the centers of two Wannier functions with different spins coincide to sufficient accuracy, the location is marked by a violet (dark gray) circle. Otherwise, spin-up and spin-down Wannier centers are shown as light red (gray) and dark blue (black) circles with an arrow. The diameter of each circle is proportional to the extent of the corresponding Wannier function. To enhance readability, the Wannier centers at the back-bonds have been dropped. Panel (d) shows plots of a spin-up and a spin-down Wannier function within the intradimer transition state. The drawing plane of these plots contains the back dimer and contour levels are drawn at 0.2, 0.1, and $0.05a_{\text{Bohr}}^{-3/2}$.

C. Hydrogen vacancy pairs

The potential energy surface of two hydrogen vacancies at the Si(001) monohydride surface (V_{2H}), i.e., of two interacting dangling bonds, is more involved than that of one vacancy due to the loss of symmetry. Therefore, this section is divided into one part covering the stable geometries and another which is concerned with diffusion pathways. Since the terms "H vacancy" and "free dangling bond" describe exactly the same physical situation at the Si(001) monohydride surface, they are used and meant synonymous in this section.

1. Vacancy configurations

The vacancies investigated in the STM study of Schwalb *et al.*[13] are not isolated from each other because H desorption from the monohydride surface takes place only molecularly. Therefore, only geometries reachable after very few hopping steps right after H_2 desorption actually occur. In order to model the physical situation encountered in experiment, we have explored the total energy landscape of two interacting vacancies in various V_{2H} configurations. We start out from configuration pattern P_3 in the center of Fig. 3. It results after molecular desorption of H_2 from a Si(001) monohydride surface by recombination of two H atoms from adjacent Si

dimers via the interdimer pathway.[2] The other relevant V_{2H} configuration patterns which we have investigated are explained in the caption of Fig. 3. Note that P_1 is the only "single dimer" configuration with both vacancies at the same dimer, which becomes buckled, therefore. This configuration is distinguished by the shortest distance between the interacting DBs among all patterns in Fig. 3 and thus exhibits by far the strongest DB interaction.

Geometries with both vacancies within the same dimer row, i.e., all patterns except P_4, have been optimized within a $c(4\times4)$ unit cell. Interrow pattern P_4 has been modeled within a larger 4×3 unit cell because in a $c(4\times4)$ cell, the resulting pattern is equivalent to the P_2 geometry. Figure 3 additionally contains the interaction energies of the two vacancies, i.e., the energy differences between the configuration at hand and a configuration containing two isolated vacancies. An additional optimization of a pattern P_7 (not shown in Fig. 3) within a 4×3 cell has yielded an interaction energy of -0.001 eV. This configuration follows by an interrow hop C of the lower vacancy of pattern P_2 in Fig. 3 to the right. Good convergence of the interaction energies has been checked by accompanying calculations employing $c(8\times4)$ unit cells.

The interaction energies are remarkably well described by a nearest-neighbor model employed by Schwalb *et al.*[11] after an original proposal from Hu *et al.*[31] This model is used to assess energy differences of configurations containing an equal number of H atoms. The basic assumption is that H vacancies (free DBs) on the monohydride surface only interact with their nearest neighbors either on the same dimer or on the next dimers along the dimer row. According to this model, the single-dimer configuration P_1 is lowered by the pairing energy ε whereas two adjacent DBs on neighboring dimers in the same row (P_3) lead to a smaller total energy gain, the clustering energy ω. For all other configurations it is assumed that the DBs do not interact because of their larger distance. Thus their energy is the same as the one of two isolated DBs. Indeed, our results show that the energies can be described to an accuracy of 0.010 eV using $\varepsilon = 0.289$ eV and $\omega = 0.042$ eV. These numbers compare very well with the experimental values of $\varepsilon = 0.319$ eV ± 0.025 eV and $\omega = 0.037$ eV ± 0.010 eV from Ref. 11.

Let us briefly address possible spin polarizations of the dangling bond configurations. At a single isolated vacancy the Si DB is half occupied by one valence electron. If there are two free DBs close to one another, their interaction may give rise to particular spin-polarization effects. Certainly, it makes a difference whether the DBs are nearest (P_1 and P_3) or more distant (the other patterns) neighbors. The single dimer without H in the P_1 configuration is buckled with an occupied DB at the up atom and an empty DB at the down atom such as a buckled dimer on the clean Si(001) surface. Thus the electronic structure of this configuration is unpolarized. In all other configurations (except P_3), the DBs are more distant and there is effectively no overlap so that the spin polarizations of the two DBs are completely independent from each other. Thus, there is a ferromagnetic configuration with both DBs polarized in the same direction, as well as an antiferromagnetic configuration with one spin-up and
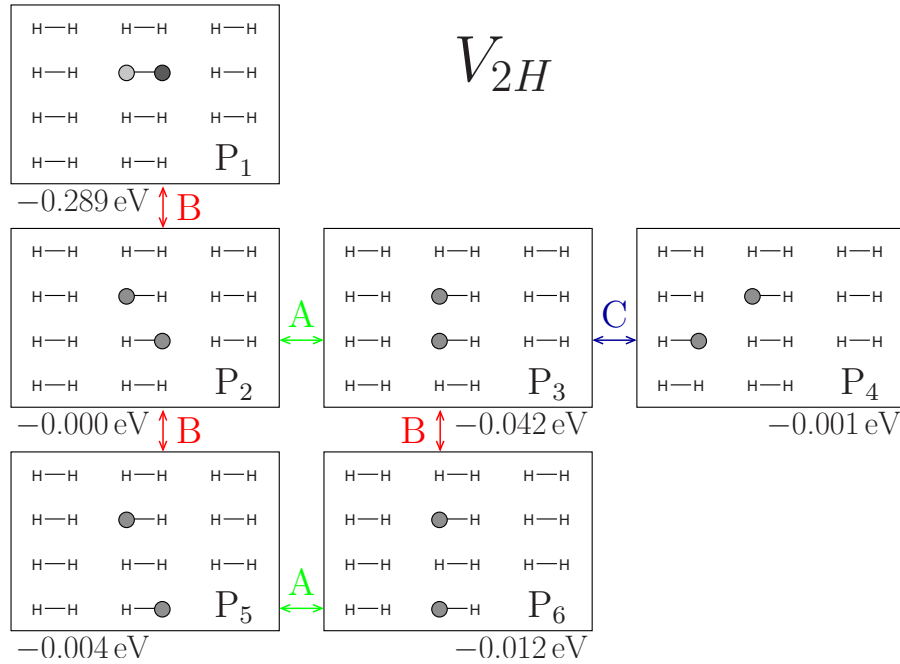
FIG. 3. (Color online) Sketches of six different V_{2H} configuration patterns P_1 to P_6 of two H vacancies on the Si(001) monohydride surface. For further details of the labeling, see caption of Fig. 1. Note that the upper H vacancy stays in a fixed (lateral) position in all six patterns while the lower one (or conversely the corresponding H atom) has to hop in order to reach a neighboring configuration. Starting from P_3, the patterns P_2, P_4, and P_6 are reached by an A, C, or B step, respectively. Patterns P_1 and P_5 result when the second vacancy hops up or down by a step B from pattern P_2. In addition, the vacancy interaction energy is given for each configuration.

one spin-down electrons. Both of these configurations are degenerate in energy. There is no significant energetic difference to two arbitrarily separated DBs, which by definition have an interaction energy of zero. As a side remark, we note that the polarization energy, i.e., the energy difference between a nonspin-polarized and a spin-polarized configuration amounts to 0.13 eV for each isolated DB.

The stable P_3 configuration, which has been studied in great detail by Lee *et al.*,[14] is special with respect to spin polarization. The authors have shown that the single-dimer configuration of two DBs (P_1) on the Si(001) monohydride surface is nonmagnetic while the P_3 configuration is antiferromagnetic. Our results are in full agreement with the findings of these authors. We also find that the stable P_3 ground state consists of two symmetric dimers with spin-polarized, antiferromagnetically coupled DBs. The coupling is responsible for the clustering of the two DBs on two neighboring dimers leading to an energy gain of $\omega = -0.042$ eV. Interestingly, the interaction energy is $+0.012$ eV in the ferromagnetic configuration which is thus even less favorable than two isolated DBs. The difference of 0.054 eV between the two magnetic states compares extremely well with the value of 0.06 eV obtained by Lee *et al.*[14] We note in passing that the energy difference between the ground state and an unpolarized, Jahn-Teller distorted geometry with buckled dimers is 0.083 eV according to our calculations while it is 0.12 eV in Ref. 14, which is also reasonably close.

2. Reaction pathways

The arrows in Fig. 3 indicate the hopping processes considered. Interestingly, the respective transition-state geom-

etries turn out to be not spin polarized. Prior to the actual transition one Si dimer atom with its free DB buckles downwards and donates its electron to the other dimer, whose DB buckles upwards in turn. This is illustrated in the following paragraphs using maximally localized Wannier functions.

Figure 4 shows the intradimer pathway A from the P_3 (right panel) to the P_2 configuration (left panel). Here, the hopping occurs on the front dimer. Both the initial P_3, as well as the final P_2 configurations are spin polarized similar to the V_H ground state in Fig. 2(a). We note in passing that our choice to show the antiferromagnetic configuration (one spin-up and one spin-down DB states) of the P_2 geometry is somewhat arbitrary as it is energetically degenerate with the corresponding ferromagnetic configuration (both DBs occupied by a spin-up Wannier function), as discussed in Sec. III C 1.

The second panel from the right shows a snapshot geometry $P_3^{(\rightarrow 2)}$ on the way from P_3 to the transition-state geometry $T_A^{(2\leftrightarrow 3)}$. Both dimers become buckled due to an electron transfer from the front dimer to the back dimer.[32] As Wannier functions span only the occupied electronic subspace, an unoccupied DB can be recognized simply by the absence of a Wannier center.

The central panel of Fig. 4 shows the transition geometry $T_A^{(2\leftrightarrow 3)}$ where the H atom is midway between the right and left Si atom. The former H-Si Wannier function is localized near the H atom and additionally participates in the Si-Si bond. Thus, there is a partial π bond between the Si dimer atoms also reflected in the contracted bond length of 2.26 Å (see first line of Table IV). Both DBs are unoccupied within the transition state. The H atom keeps this electron pair fur-
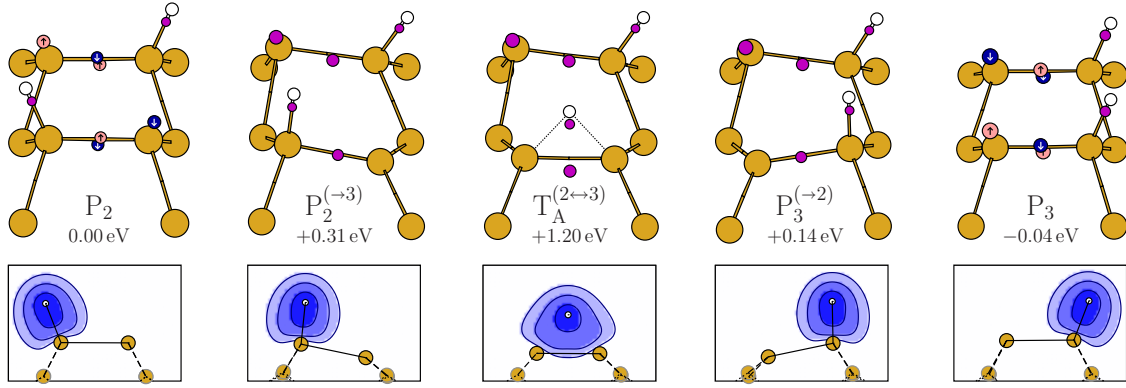
FIG. 4. (Color online) Geometries and maximally localized Wannier functions along the intradimer pathway A between P_3 (right) and P_2 (left). The top panels show a bird's eye view as described in the caption of Fig. 2. The bottom panels show plots of the Wannier function which is localized at the moving H atom of the front dimer. These plots are described in the caption of Fig. 2.

ther along its path through $P_2^{(\to 3)}$ to configuration P_2. In the last step, one electron from the back DB is transferred to the front DB, making both spin-polarized again.

In total, one electron is transferred to the DB of the adjacent dimer at the beginning of this diffusion step and the H atom keeps a complete electron pair along the whole reaction path. This additional charge at the H atom is used to build up a partial π bond between the Si dimer atoms within the transition state. This mechanism leads to a significantly lower energy barrier than a spin-polarized pathway.

The intrarow and interrow pathways follow another mechanism that differs from the intradimer reaction pathway described above. Figure 5 exemplifies this with the first half of an interrow hop (C) from P_3 to P_4. The top panel shows a section of the P_3 geometry with two dimers of adjacent rows featuring a singly occupied DB on the right dimer. The $P_3^{(\to 4)}$ geometry is similar to the $P_3^{(\to 2)}$ geometry of the intradimer transition P_3 to P_2 in that the dimer buckles upwards and the respective DB becomes fully occupied due to an electron transfer from the DB of the adjacent dimer in the same row (not shown in Fig. 5). Together with the Si-H bond on the left dimer, this sums up to two electron pairs in the Si-H-Si bridge of the transition state $T_C^{(3\leftrightarrow 4)}$. The rest of the reaction pathway would essentially be a mirrored version of the $P_3^{(\to 4)}$ and P_3 panels and is therefore not shown in Fig. 5.

Thus, actually only a proton is transferred from the doubly occupied DB of the left dimer to the doubly occupied DB of the right dimer, leaving the electron pairs basically in

place. This way, the proton can be screened more effectively compared to a spin-polarized transition state like in the V_H case, which would comprise one electron less within the Si-H-Si bridge. The intrarow hop follows the same reaction mechanism and is thus not further discussed, here. These two types of hopping differ from the intradimer pathway because there is no dimer bond to which a concomitant electron pair can contribute a partial π bond. In Table IV we summarize the structural parameters for the transitions states of a number of hopping processes indicated in Fig. 3, some of which have been discussed in more detail above.

The vacancy interaction energies E_t, E_i, and E_f in the transition-, initial-, and final-state geometries, respectively, are summarized in Table V. The barrier for a particular hopping process depends on the direction of the hop. Changing the hopping direction interchanges E_i and E_f of the process. Therefore, Schwalb *et al.*[11] have defined an effective barrier

TABLE IV. Structural parameters (as in Table I, see caption for details) but for H diffusion on Si(001) monohydride with two vacancies (V_{2H}). The two H-Si distances in each transition geometry differ slightly and the shorter one is given.

		d_{di}	$d_{H\text{-}Si}$	$d_{Si\text{-}Si}$
V_{2H}	$T_A^{(3\to 2)}$	2.26 (2.41)	1.78 (1.50)	2.26 (2.41)
	$T_B^{(3\to 6)}$	2.43 (2.41)	1.85 (1.50)	3.23 (3.84)
	$T_B^{(2\to 1)}$	2.40 (2.40)	1.84 (1.50)	3.28 (3.85)
	$T_C^{(3\to 4)}$	2.63 (2.41)	2.06 (1.50)	4.12 (5.29)
	$T_C^{(2\to 7)}$	2.63 (2.40)	2.04 (1.50)	4.04 (5.31)

FIG. 5. (Color online) Geometries and Wannier centers along the first half of the V_{2H} interrow pathway (c) from P_3 to P_4. For further details of the presentation see the caption of Fig. 2. The second DB of the P_3 geometry is not shown in this figure. It buckles downward in the $P_3^{(\to 4)}$ geometry essentially in the same way as the front dimer in the $P_3^{(\to 2)}$ geometry of Fig. 4.

TABLE V. Interaction energies E_i, E_t, and E_f (in eV) of the initial, transition, and final geometries along different hopping pathways of the second vacancy. The last column denotes the effective barrier height ΔE_{eff} defined in the text.

Path	Hop	E_i	E_t	E_f	ΔE_{eff}
$P_3 \rightarrow P_2$	A	-0.042	1.198	0.000	1.22
$P_2 \rightarrow P_1$	B	0.000	1.378	-0.289	1.52
$P_3 \rightarrow P_6$	B	-0.042	1.529	-0.012	1.56
$P_3 \rightarrow P_4$	C	-0.042	2.130	-0.001	2.15
$P_2 \rightarrow P_7$	C	0.000	2.154	-0.001	2.16

$\Delta E_{\text{eff}} = E_t - (E_i + E_f)/2$ as the difference between the energy of the transition state and the average of the initial- and final-state energies in order to determine more meaningful barrier energies. The resulting effective barriers are given in the last column of Table V. From these numbers, average effective barriers of 1.22 eV, 1.54 eV, and 2.15 eV follow for A, B, and C hopping of one vacancy, respectively, which will be referred to as activation energies ΔE_{act} of the V_{2H} system. They are the most meaningful reference values for comparison to activation energies of the H and V_H systems. Additionally, this definition matches the one by Schwalb *et al.* in Refs. 11 and 13. Therefore, resulting experimental and theoretical hopping rates can directly be compared.

IV. DISCUSSION

A. Barrier energies

To ease the identification of salient trends, we have plotted in Fig. 6 the heights of the activation barriers for intradimer (A), intrarow (B), and interrow (C) diffusion in the H, V_H, and V_{2H} systems versus the distances $d_{\text{H-Si}}$ and $d_{\text{Si-Si}}$ from Tables I, III, and IV. In the latter case, average values have been used for clarity.

First, the figure highlights that interrow diffusion C has the highest activation barrier of all three investigated systems. This is a direct consequence of the very large distance $d_{\text{Si-Si}}$ of the two Si atoms in the transition state between which H has to hop in an interrow transition step. Interrow processes are least likely to occur, therefore.

Second, for any type of diffusion (A, B, or C), the monohydride surface with a single vacancy (V_H system) has the highest barrier, as compared to the other two systems (H, V_{2H}). This means that the V_H system is the most rigid among all three.

Third, the difference in activation energy between the V_H and V_{2H} systems is roughly 0.2 eV for all three types of diffusion. It reveals a larger flexibility of the V_{2H} system for hydrogen diffusion, as compared to the V_H system. The reason for this fact is as follows. The additional degree of freedom of the charge transfer in the V_{2H} system, described in Sec. III C, increases the charge density in the vicinity of the moving proton for intrarow (B) and interrow (C) transitions. The enhanced screening of the proton then lowers the transition energy by about 0.2 eV in both cases. This mechanism is not in operation for intradimer diffusion (A) where the screening is a relatively minor issue due to the presence of

the dimer bond. Here, the energy is lowered by 0.2 eV compared to the respective V_H barrier because of the partial π bond within the transition state.

Fourth, an isolated hydrogen atom on a clean Si(001) surface (H) and an isolated hydrogen vacancy in a Si(001) monohydride surface (V_H) are complementary but inequivalent. Figure 6, as well as Tables I and III, show that the activation energies of the H and V_H systems are similar for intradimer hopping (within 0.04 eV). This is because the atomic configurations of the relevant dimers are essentially the same, as can also be seen from the corresponding geometry parameters. On the other hand, the activation energies of H and V_H become more different for intrarow hopping (by 0.18 eV) and differ most for interrow hopping (by 0.25 eV). This is closely related to the huge difference of 0.39 Å in $d_{\text{Si-Si}}$ between H and V_H. The reason is mainly that the dimer
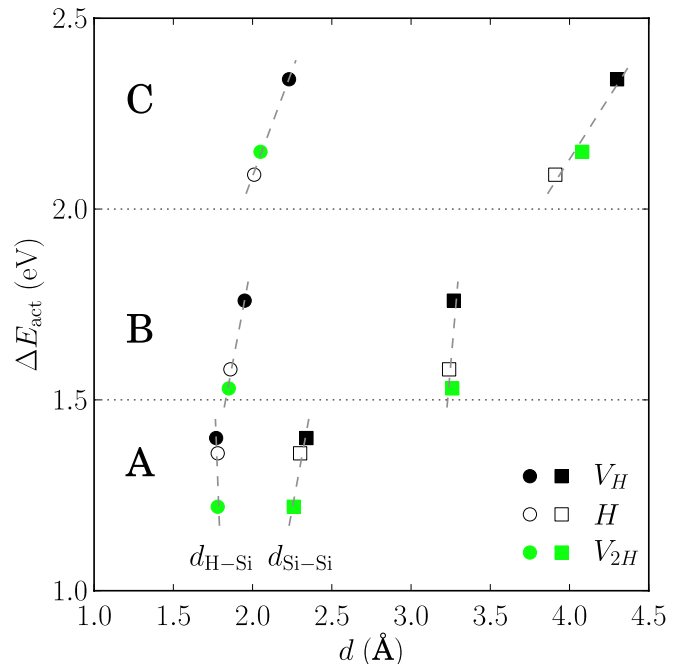
FIG. 6. (Color online) Barrier energies ΔE_{act} for (a) intradimer, (b) intrarow, and (c) interrow hydrogen diffusion on the clean surface (H) and the monohydride surface with one (V_H) or two (V_{2H}) vacancies as a function of distances $d_{\text{H-Si}}$ (circles) and $d_{\text{Si-Si}}$ (squares) characterizing the transition states (cf. caption of Table I). For each combination of a particular diffusion step and distance type, a local linear fit is added as a guide to the eye.

TABLE VI. Activation energies ΔE_{act} (in eV) and pre-exponential factors ν^* (in 10^{14} s^{-1}) for intradimer (A), intrarow (B), and interrow (C) hopping of one H atom on the clean Si(001)-(2×1) surface (H) and on the Si(001)-(2×1) monohydride surface with one (V_H) or two paired (V_{2H}) vacancies.

System	H		V_H		V_{2H}	
Hop	ΔE_{act}	ν^*	ΔE_{act}	ν^*	ΔE_{act}	ν^*
A	1.36	1.4	1.40	1.0	1.22	0.3
B	1.58	1.0	1.76	0.8	1.54	1.3
C	2.09	11.0	2.34	2.3	2.15	2.9

buckling within the stable H geometry shortens the distance between two adjacent up atoms on different rows to 5.14 Å compared to 5.29 Å on a monohydride surface. In the respective transition geometry the dimers tilt even further and thus shorten the corresponding distance and additionally reduce the activation energy. In view of the exponential dependence of the hopping rate on the activation energy ΔE_{act}, a difference of 250 meV is quite substantial.

B. Hopping rates

So far, we have only reported activation energies while only hopping rates are directly accessible in STM experiments. In order to compare our results in a more meaningful way to experimental data, we have calculated hTST attempt frequencies ν^* in addition to the activation energies (tabulated in Table VI). Using the Arrhenius formula

$$\Gamma = \nu^* e^{-\Delta E_{act}/k_B T}$$

theoretical hopping rates can be deduced. As we are not aware of any experimental studies on the diffusion of isolated vacancies (V_H), we restrict the following discussion to isolated hydrogen atom (H) and paired vacancy (V_{2H}) systems.

Before we actually compare the calculated hopping rates to experimental values, we recall that transition rates are extremely sensitive to changes in the activation energies ΔE_{act} due to the exponential dependency. A change in the activation energy by 0.12 eV at 600 K at a constant prefactor ν^* changes the hopping rate by a power of 10. Unfortunately, GGA barrier energies are often not more accurate than 0.1 eV on an absolute scale due to systematic errors.[33] On the other hand, transitions can occur on time scales ranging from about 10^{-14} s up to arbitrary large times (which correspond to barriers impenetrable at a given temperature). Most often one is only interested in an estimate of the order of magnitude, i.e., whether a given process is much faster than, much slower than, or roughly within the time scale of interest. Therefore, theoretically predicted hopping rates are actually quite useful quantities.

It is apparent from Table VI that the attempt frequency of the H interrow transition is extraordinarily large. This cannot solely be explained by invoking the general notion that attempt frequencies tend to get larger with increasing barrier heights. The large prefactor for process C in the H system points to a very flat dependence of the total energy on the H coordinates perpendicular to the interrow path direction. It

turns out, however, that the product of the corresponding two vibrational frequencies is only about 30% smaller in the interrow transition state compared to the other two transition states. It is reasonable to assume, instead, that the large prefactor is somehow connected to the fact that the H interrow transition state T_C is actually semimetallic while all other transition states studied in this work are semiconducting.

Figure 7 shows an Arrhenius diagram of the hopping rate Γ versus inverse temperature $1/T$. For temperatures below about 1800 K the magnitude of the hopping rates mainly depends on the barrier energies. Thus, the rates get smaller from intradimer (A) through intrarow (B) to interrow (C) hoppings. The two lines for the H and V_{2H} systems belonging to one type of hopping A, B, or C, respectively, group together because the activation barriers are similar in each
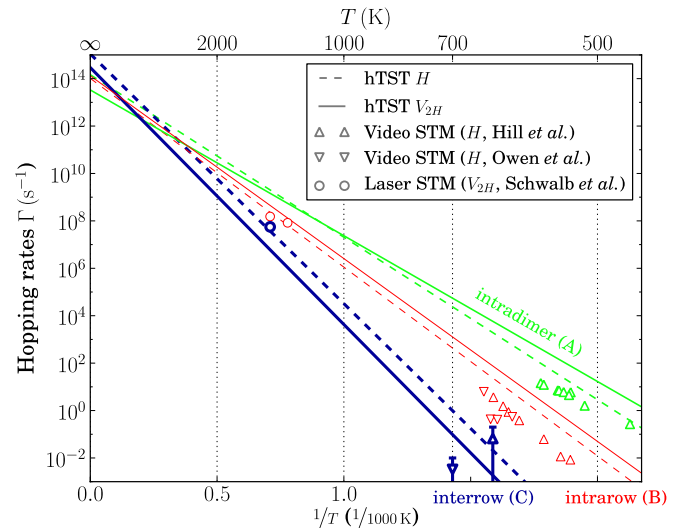
FIG. 7. (Color online) Arrhenius diagram of hopping rates Γ. The lines are calculated hTST transition rates for paired H vacancies on a monohydride surface (V_{2H}, solid) as well as for isolated H atoms on clean Si(001) (H, dashed). Intradimer, intrarow, and interrow hopping rates are shown in green (bright gray), thin red (gray), and fat blue (dark gray), respectively. The circles (○) denote experimental high temperature V_{2H} intrarow and interrow data points from Schwalb *et al.* (Refs. 11 and 13). The video STM data at low coverage (H) of the groups of Ganz (Ref. 9) and Briggs (Refs. 7 and 10) are shown by triangles (Δ and ∇, respectively). The blue (dark gray) error bars with triangles denote upper limits for moderate temperature H interrow hopping rates based on the data of Hill *et al.* (Ref. 9) (at 630 K) and Bowler *et al.* (Ref. 10) (at 700 K) as described in the text.

case. Note that eighteen orders of magnitude of Γ are plotted in Fig. 7.

Within the temperature regime below 700 K, video STM results of Owen *et al.*[7] (∇) as well as of Hill *et al.*[9] (Δ) for hydrogen intradimer (A) and intrarow (B) diffusion have been added. The absolute values of the measured and calculated hopping rates deviate at most by a factor of ten. More importantly, the slopes of the respective Arrhenius plots (dashed lines for A and B), as calculated for the *H* system, show encouraging agreement with experiment over a larger temperature range. The agreement is very good for intrarow hopping (B) where the calculated transition barrier height of 1.58 eV deviates from the experimentally determined value of 1.75 eV (see Table II) only by 0.17 eV. Here the slopes of the calculated line and the data are very similar and there is only an offset on an absolute scale. In case of intradimer hopping (A), the difference of the calculated (1.36 eV) and experimentally determined (1.01 eV) barrier height of 0.35 eV is larger by a factor of two. As a consequence, the corresponding slopes of the calculated and measured Arrhenius plots show appreciable deviations. Nevertheless, there is reasonable general agreement between theory and experiment for hopping processes A and B.

Figure 7 additionally contains the hopping rates for intrarow diffusion around 1400 K (thin circles) as obtained by Schwalb *et al.*[11] from heating the Si(001) monohydride surface to these temperatures for a few nanoseconds using a laser pulse. It can be compared to the solid V_{2H} line, which slightly overestimates the experimental data points. Thus, if one keeps in mind the strong dependence of the hopping rates on the barrier energy, the calculated intradimer and intrarow hopping rates agree quite well with experimental results both in the moderate- and high-temperature regimes. The slight systematic overestimation of hopping rates can be attributed to the general observation that the GGA tends to underestimate the barriers of chemical reactions.[33]

As the barrier energy for interrow hops is rather large, these reactions hardly occur within the time scales feasible for video STM and there are only rough estimates for the corresponding temperature range. Schwalb *et al.*[13] deduce from the absence of any interrow observations by Hill *et al.*[9] that the rate at 630 K must be below 0.2 s^{-1} as indicated by an error bar in Fig. 7. The dashed hTST curve for the *H* system lies well within this region. The second error bar at 700 K stems from an estimation of Bowler *et al.*[10] who tracked an H atom which was trapped between two defects within a dimer row. When the authors occasionally observed the hydrogen atom to vanish, they assumed that it had performed an interrow hop. As this is reported to occur on time scales larger than 100 s, an upper boundary on the rates of 0.01 s^{-1} follows. The calculated rates for the *H* system are significantly larger but in any case support the notion that interrow events should be observable under the given experimental conditions.

Recently, Schwalb *et al.*[13] have applied their nanosecond laser technique to study interrow diffusion of H vacancies. The resulting hopping rate at 1400 K is added to Fig. 7 as a (fat) circle which lies above the corresponding solid hTST interrow hopping rate line by roughly one power of 10. Again, our results are consistent with the occurrence of interrow hopping at the given temperatures, although the actual rates differ quantitatively.

The difference between theoretical and experimental interrow hopping rates is not unreasonably large. Yet, the agreement is worse compared to the other two hopping kinds, which are particularly well described with our hTST hopping rates. Moreover, the hTST hopping rates overestimate the experimental results in the low coverage, low *T* range whereas the high coverage, high *T* data point of Schwalb *et al.*[13] is underestimated. On the other hand, one has to keep in mind that there are only very few experimental interrow data points and the low *T* values are just rough estimates. Therefore, further experimental investigations of H interrow hopping on Si(001)-(2×1) appears to be rewarding in the light of the results presented in this work. In addition, the exponential sensitivity of the hopping rates on relatively small changes of activation energies calls for more accurate calculations of interrow barriers beyond GGA, e.g., by employing quantum Monte Carlo calculations, as has been done by Filippi *et al.*[34] in their study of molecular hydrogen adsorption on and desorption from the Si(001) surface.

V. SUMMARY

We have performed a comparative *ab initio* study of H diffusion on the flat Si(001) surface both for very low and very high H coverage. Hydrogen transitions within a dimer, along a dimer row, and perpendicular to a dimer row have been investigated. The barrier energy crucially depends on the distance between the two Si neighbors of the diffusing H atom in the transition state and is thus mainly determined by the type of hopping. It is smallest for intradimer and largest for interrow hops, leaving intrarow in between in all cases.

In the case of isolated vacancies on the monohydride surface (V_H), the transferred proton is effectively accompanied by a single electron. If there is a second vacancy on a neighboring dimer in a V_{2H} system, the first step of the hopping reaction is a charge transfer from one dimer to the other, leading to buckled dimers and an unpolarized electronic state. Subsequently, in the case of an intradimer transition, the proton is accompanied by an electron pair, which partially constitutes a Si-Si dimer π bond in the transition geometry, and both DBs are unoccupied. In contrast, only the proton is transferred for intrarow and interrow hops, screened by two stretched and fully occupied Si DBs.

The activation barriers are up to 0.25 eV larger within the high coverage V_H limit, as compared to the low coverage *H* limit due to differences in the surface relaxation. Thus, a clean Si(001) surface with one adsorbed H atom and a Si(001) monohydride surface with one H vacancy are complementary but quantitatively inequivalent systems. Interestingly, for two interacting vacancies (V_{2H}) on a monohydride surface the hopping barriers for H are lowered by 0.2 eV compared to V_H due to electron-transfer processes.

We have additionally calculated hopping rates within the harmonic approximation to transition state theory. For in-

tradimer and intrarow diffusion the calculated rates agree very well with experiment both for high and moderate temperatures. Concerning interrow diffusion, our results for the hopping rates in general corroborate the occurrence of such processes under the given experimental conditions. However, there remain quantitative differences which call for further experimental and theoretical studies on this particular aspect.

ACKNOWLEDGMENTS

*Present address: Fritz-Haber-Institut der Max-Planck-Gesellschaft, 14195 Berlin, Germany; wieferink@fhi-berlin.mpg.de

[1] J. M. Jasinski and S. M. Gates, Acc. Chem. Res. **24**, 9 (1991).

[2] W. Brenig and E. Pehlke, Prog. Surf. Sci. **83**, 263 (2008).

[3] A. Vittadini, A. Selloni, and M. Casarin, Surf. Sci. Lett. **289**, L625 (1993).

[4] C. J. Wu, I. V. Ionova, and E. A. Carter, Phys. Rev. B **49**, 13488 (1994).

[5] P. Nachtigall and K. D. Jordan, J. Chem. Phys. **102**, 8249 (1995).

[6] U. Hansen and P. Vogl, Phys. Rev. B **57**, 13295 (1998).

[7] J. H. G. Owen, D. R. Bowler, C. M. Goringe, K. Miki, and G. A. D. Briggs, Phys. Rev. B **54**, 14153 (1996).

[8] M. McEllistrem, M. Algeier, and J. J. Boland, Science **279**, 545 (1998).

[9] E. Hill, B. Freelon, and E. Ganz, Phys. Rev. B **60**, 15896 (1999).

[10] D. R. Bowler, J. H. G. Owen, C. M. Goringe, K. Miki, and G. A. D. Briggs, J. Phys.: Condens. Matter **12**, 7655 (2000).

[11] C. H. Schwalb, M. Lawrenz, M. Dürr, and U. Höfer, Phys. Rev. B **75**, 085439 (2007).

[12] M. Dürr, A. Biedermann, Z. Hu, U. Höfer, and T. F. Heinz, Science **296**, 1838 (2002).

[13] C. H. Schwalb, M. Dürr, and U. Höfer, Phys. Rev. B **80**, 085317 (2009).

[14] J. Y. Lee, J. H. Choi, and J. H. Cho, Phys. Rev. B **78**, 081303 (2008).

[15] P. Hohenberg and W. Kohn, Phys. Rev. **136**, B864 (1964).

[16] W. Kohn and L. J. Sham, Phys. Rev. **140**, A1133 (1965).

[17] J. P. Perdew and Y. Wang, Phys. Rev. B **45**, 13244 (1992).

[18] L. Kleinman and D. M. Bylander, Phys. Rev. Lett. **48**, 1425 (1982).

[19] In structure and path optimizations, decay coefficients in atomic units (a_{Bohr}^{-2}) of 0.15, 0.45, and 2.50 for adlayer H atoms, 0.18, 0.50, and 1.00 for surface Si atoms, 0.20 and 0.60 for substrate Si atoms, and 0.35 for saturation layer H atoms have been used.

[20] For interaction energy calculations, adlayer H atoms and surface Si atoms are modeled using decay coefficients of 0.10, 0.23, 0.55, 1.28, 3.00 and 0.07, 0.15, 0.37, 0.85, 2.00, respectively (in atomic units). To enhance the condition of the overlap matrix, the s^* orbitals of the 0.10 shell for H are dropped.

[21] J. Wieferink, P. Krüger, and J. Pollmann, Phys. Rev. B **74**, 205311 (2006).

[22] S. K. Burger and W. Yang, J. Chem. Phys. **124**, 054109 (2006).

[23] G. Henkelman, B. P. Uberuaga, and H. Jónsson, J. Chem. Phys. **113**, 9901 (2000).

[24] P. Császár and P. Pulay, J. Mol. Struct. **114**, 31 (1984).

[25] O. Farkas and H. B. Schlegel, Phys. Chem. Chem. Phys. **4**, 11 (2002).

[26] R. Lindh, A. Bernhardsson, G. Karlström, and P.-Å. Malmqvist, Chem. Phys. Lett. **241**, 423 (1995).

[27] G. H. Vineyard, J. Phys. Chem. Solids **3**, 121 (1957).

[28] N. Marzari and D. Vanderbilt, Phys. Rev. B **56**, 12847 (1997).

[29] A. A. Mostofi, J. R. Yates, Y.-S. Lee, I. Souza, D. Vanderbilt, and N. Marzari, Comput. Phys. Commun. **178**, 685 (2008).

[30] J. Wieferink, P. Krüger, and J. Pollmann, Phys. Rev. B **78**, 165315 (2008).

[31] Z. Hu, A. Biedermann, E. Knoesel, and T. F. Heinz, Phys. Rev. B **68**, 155418 (2003).

[32] We like to note that the actual charge transfer cannot be studied by a continuous motion of Wannier centers because the electronic structure is metallic somewhere on the pathway between P_3 and $P_3^{(\rightarrow 2)}$. This can be understood by the fact that the spin-down DB band of the down atom rises in energy along the pathway while the spin-up DB band at the up atom lowers until they cross.

[33] A. J. Cohen, P. Mori-Sanchez, and W. Yang, Science **321**, 792 (2008).

[34] C. Filippi, S. B. Healy, P. Kratzer, E. Pehlke, and M. Scheffler, Phys. Rev. Lett. **89**, 166102 (2002).

[35] M. J. Litzkow, M. Livny, and M. W. Mutka, *Condor—A Hunter for Idle Workstations*, in Proceedings of the 8th International Conference on Distributed Computing Systems (IEEE Comput. Sci. Press, Washington, DC, 1988), pp. 104–111.